J. Fluid Mech. (1999), *vol.* 388, *pp.* 315–334. Printed in the United Kingdom

Stability of multiple steady states of convection in laterally heated cavities

By A. Yu. GELFGAT, P. Z. BAR-YOSEPH AND A. L. YARIN

Computational Mechanics Laboratory, Faculty of Mechanical Engineering,
Technion – Israel Institute of Technology, Haifa 32000, Israel
e-mail: merbygr@cmlp.technion.ac.il

(Received 24 September 1997 and in revised form 28 December 1998)

A parametric study of multiple steady states, their stability, onset of oscillatory instability, and some supercritical unsteady regimes of convective flow of a Boussinesq fluid in laterally heated rectangular cavities is presented. Cavities with four no-slip boundaries, isothermal vertical and perfectly insulated horizontal boundaries are considered. Four distinct branches of steady-state flows are found for this configuration. A complete study of stability of each branch is performed for the aspect ratio A (length/height) of the cavity varying continuously from 1 to 11 and for two fixed values of the Prandtl number: $Pr = 0$ and $Pr = 0.015$. The results are represented as stability diagrams showing the critical parameters (critical Grashof number and the frequency at the onset of the oscillatory instability) corresponding to transitions from steady to oscillatory states, appearance of multi-roll states, merging of multiple states and backwards transitions from multi-roll to single-roll states. For better comparison with the existing experimental data, an additional stability study for varying Prandtl number ($0.015 \leqslant Pr \leqslant 0.03$) and fixed value of the aspect ratio $A = 4$ was carried out. It was shown that the dependence of the critical Grashof number on the aspect ratio and the Prandtl number is very complicated and a very detailed parametric study is required to reproduce it correctly. Comparison with the available experimental data for $A = 4$ shows that the results of a two-dimensional stability analysis are in good agreement with the experimental results if the width ratio (width/height) of the experimental container is sufficiently large. The study is carried out numerically with the use of two independent numerical approaches based on the global Galerkin and finite-volume methods.

1. Introduction

The motivation of the present work is manufacture of bulk semiconductor crystals. Hurle (1966) showed that the convective oscillations caused striations in crystals growing from melts. Accordingly, the problem of onset of oscillatory instability of steady convective flows has been extensively studied. Recent studies have shown that convection in the liquid phase strongly affects the processes of crystal growth from melt (Müller & Ostrogorsky 1994). The simplest geometry among several crystal growth technologies has the horizontal configuration of the Bridgman method (Dupret & Van der Bogaert 1994; Monberg 1994), where the convective flow is induced by the horizontal component of the temperature gradient. The simplest model of the convective flow in the horizontal Bridgman crystal growth device is the flow in a

laterally heated rectangular cavity (see Henry & Buffat 1998, and references therein). This model has been intensively studied both experimentally and numerically, and is used as a convenient benchmark problem for particular values of the aspect ratio and the Prandtl number (GAMM Workshop: Roux 1990).

Recent experimental (Braunsfurth & Mullin 1996) and numerical (Gelfgat, Bar-Yoseph & Yarin 1997, 1998*a–c*) studies showed that the transition from steady to oscillatory state in these flows strongly depends on the Prandtl number and the aspect ratio. However, most of the numerous numerical studies of this problem consider fixed values of these parameters, which usually coincide with those used in the GAMM benchmark (Roux 1990), $A = 4$ and $Pr = 0$ or 0.015. There are very few numerical works where other values of the aspect ratio or Prandtl number were considered in the context of crystal growth from melts. At the same time, there is no common understanding of the dependence of the critical Grashof number on the aspect ratio of the cavity and the Prandtl number. Gelfgat *et al.* (1997) considered cavities with a stress-free upper boundary and obtained the dependence $Gr_{cr}(A)$ for the whole interval $1 \leqslant A \leqslant 10$ and for the two fixed Prandtl number values, 0 and 0.015. It was shown that the dependence $Gr_{cr}(A)$ is non-monotonic and contains hysteresis loops, such that stability properties of the flow at close values of the aspect ratio can be surprisingly different. A similar study for the case of four no-slip boundaries seems to be a minor addition. However, this case appears to be much more interesting, as well as much more complicated, because of the existence of multiple stable steady-state flows (Crespo del Arco, Pulicani & Randriamampianina 1989; Gelfgat *et al.* 1998 *a, b*). For $A > 4$, several (more than two) steady states can coexist simultaneously, such that the resulting asymptotic state is determined not only by the governing parameters but also by the initial conditions. To complete the stability diagram, the stability boundaries should be calculated for each branch of multiple steady states separately. The corresponding curves $Gr_{cr}(A)$ have a complicated shape, such that several hundred points have to be calculated to complete the stability diagram. This is carried out in the present study for the interval $1 \leqslant A \leqslant 10$, and for cavities with four no-slip walls. To the best of our knowledge these stability diagrams are reported here for the first time.

There exists an expectation that the case of $Pr = 0$, corresponding to infinite thermal diffusivity, might be a plausible model for any $Pr = O(10^{-2})$ which is characteristic of semiconductor crystal growth from melts. If this were true, the stability analysis could be simplified by excluding the convective thermal effects (at $Pr = 0$, instability is purely hydrodynamic). A conclusion about similarity between small and zero Prandtl numbers is usually made for a single value of the aspect ratio and a single non-zero value of the Prandtl number ($Pr = 0$ and 0.015 for $A = 4$ in Gelfgat & Tanasawa 1994; Henry & Buffat 1998). This, however, is not the case, since, as is shown here, the case with $Pr = 0$ can never be used to model any real semiconductor crystal growth process. It is shown that the occasional similarity, corresponding to the mentioned values of Pr and A, disappears at $Pr \approx 0.023$ and does not exist at all if other values of the aspect ratio or other branches of steady-state flows are considered. It is shown also that the end effects cannot be neglected when oscillatory instability in long cavities is studied.

Recently, most studies on the oscillatory instability of convective flows considered two-dimensional flow models only. Several three-dimensional numerical investigations involving small Prandtl numbers, used rather coarse grids. The finest three-dimensional grid ($120 \times 60 \times 60$) was used by Babu & Korpela (1994), but even then it was impossible to reproduce completely the experimental results of Pratte

& Hart (1990). Convergence studies for the two-dimensional model (summarized in Roux 1990; see also § 2.3) showed that higher-order methods and/or finer grids may be needed for accurate unsteady calculations in the vicinity of the critical points. Three-dimensional unsteady calculations are CPU-time consuming, and impracticable for parametric studies. By contrast, two-dimensional parametric stability analysis provides important information on the dependence of stability properties of the flow on the governing parameters, which is necessary for future experiments and three-dimensional numerical modelling. On the basis of the present results, it is possible to foresee an existence of multiple many-roll steady states in three-dimensional laterally heated cavities. Such multiple states have not been reported previously. It will also be shown (see § 4.3) that, with some restrictions, the results of a two-dimensional study are comparable with experimental findings.

Thermal boundary conditions, used in the present study, are chosen in accordance with several experimental studies (see § 4.3), where the vertical boundaries were kept at constant temperatures and the horizontal boundaries were reported to be good thermal insulators. To compare with the experimental results obtained for different Prandtl numbers, it was necessary to calculate the dependence $Gr_{cr}(Pr)$. The aspect ratio was fixed at $A = 4$, which is common for most of the experiments. It is shown that the curve $Gr_{cr}(Pr)$ contains several hysteresis loops in the narrow interval $0.023 < Pr < 0.027$. This dependence provides a qualitative explanation of the recent experimental results of Braunsfurth & Mullin (1996) and is reported here for the first time.

The article is organized as follows. Section 2 contains the formulation of the problem. Some relevant peculiarities of the numerical methods involved are presented in § 3. Results and a discussion are presented in § 4. The conclusions are drawn in § 5.

2. Formulation of the problem

The convective flow of a Boussinesq fluid with kinematic viscosity v^* and thermal diffusivity χ^* in a cavity of length L^* and height H^* is considered. The vertical boundaries of the cavity have constant temperatures θ^*_{hot} and θ^*_{cold}, while the horizontal ones are perfectly thermally insulated. All four boundaries are rigid (no-slip velocity conditions imposed). This set of boundary conditions corresponds to the *Ra-Ra* benchmark case defined in Roux (1990). The flow is described by the momentum, continuity and energy equations in a Cartesian coordinate system (x^*, y^*). Using the scales $H^*, H^{*2}/v^*, v^*/H^*, \rho^*(v^*/H^*)^2$ for length, time, velocity and pressure, respectively, and $\theta = (\theta^* - \theta^*_{cold})/(\theta^*_{hot} - \theta^*_{cold})$ for non-dimensionalization of the temperature, the set of Boussinesq equations for the non-dimensional velocity $\boldsymbol{v} = \{v_x, v_y\}$, temperature θ and pressure p in the rectangular domain $0 \leqslant x \leqslant A$, $0 \leqslant y \leqslant 1$ is

$$\frac{\partial \boldsymbol{v}}{\partial t} + (\boldsymbol{v} \cdot \nabla)\boldsymbol{v} = -\nabla p + \Delta \boldsymbol{v} + Gr\ \theta\ \boldsymbol{e}_y, \tag{1}$$

$$\frac{\partial \theta}{\partial t} + (\boldsymbol{v} \cdot \nabla)\theta = \frac{1}{Pr}\Delta\theta, \tag{2}$$

$$\nabla \cdot \boldsymbol{v} = 0. \tag{3}$$

Here $A = L^*/H^*$ is the aspect ratio of the cavity, $Gr = g^*\beta^*(\theta^*_{hot} - \theta^*_{cold})H^{*3}/v^{*2}$ the Grashof number, $Pr = v^*/\chi^*$ the Prandtl number, g^* acceleration due to gravity in the y-direction, β^* the thermal expansion coefficient, and $\boldsymbol{e}_y$ the unit vector in the vertical direction.

The no-slip boundary conditions are imposed at all boundaries

$$v_x = v_y = 0 \quad \text{at} \quad x = 0, A, \quad y = 0, 1, \tag{4}$$

constant temperatures are prescribed at the vertical boundaries

$$\theta = 1 \quad \text{at} \quad x = 0, \quad \theta = 0 \quad \text{at} \quad x = A, \tag{5}$$

with zero heat flux through the horizontal boundaries

$$\partial\theta/\partial y = 0 \quad \text{at} \quad y = 0, 1. \tag{6}$$

3. Numerical procedures and test calculations

3.1. *Numerical methods*

The problem (1)–(6) is solved using two independent numerical approaches. The Global Galerkin method was used for analysis of stability of steady flows and weakly nonlinear analysis of slightly supercritical oscillatory states. Details on the basis functions and numerical stability analysis can be found in Gelfgat & Tanasawa (1994). More details on the weakly nonlinear asymptotic approximation of slightly supercritical flows are given in Gelfgat, Bar-Yoseph & Solan (1996*a*).

Solution of the full unsteady problem is carried out by the finite-volume method, based on the SIMPLE algorithm (Patankar & Spalding 1972), with second-order three time-levels approximation of the time derivative (Janssen, Henkes & Hoogendoorn 1993). The finite-volume method is used for three main purposes: validation of the stability results obtained by the Galerkin method, calculation of the supercritical unsteady flows for large supercriticalities, and calculations in cases of subcritical bifurcations. The finite-volume method provides conservative numerical schemes (for conservation of mass, momentum, and heat), which is very important for the numerical study in the vicinity of critical stability points. For this reason, it is chosen for the present unsteady calculations.

Combination of two independent numerical approaches allows for verification of the results obtained, especially in the cases where multiple steady solutions and complicated stability diagrams occur.

3.2. *Test calculations*

Detailed test calculations are reported here for $A = 4$, which is the most common case, and for $A = 1$, for which independent numerical data are available in literature. Convergence of the steady states under the Galerkin method has already been studied by Gelfgat & Tanasawa (1994). In the present paper, a convergence study for the critical parameters (critical Grashof number and critical frequency) is reported. Additional comparisons of the results obtained by the Galerkin and finite-volume methods are presented in § 4.

The convergence study and the comparison with other numerical results for a square cavity $A = 1$ are given in table 1, which shows that starting with 26×26 functions ($N_x \times N_y = M_x \times M_y = 26 \times 26$), two digits of both critical parameters (Gr_{cr} and $f_{cr} = \omega_{cr}/2\pi$) remain unchanged, whereas three digits remain unchanged when 36×36 functions are used. Unfortunately, the available independent results (Esposito & Behnia 1992; Bergman & Ball 1994) are obtained on rather coarse grids, so that only a qualitative comparison is possible.

A more rigorous comparison can be effected for $A = 4$. In this case, two branches of steady states exist for $Pr = 0.015$ and three branches for $Pr = 0$ (see figure 1 and

		20×20 basis functions	26×26 basis functions	30×30 basis functions	36×36 basis functions	40×40 basis functions	Bergman & Ball (1994) 33×33 collocation points	Esposito & Behnia (1992) 64×64 finite-difference stretched grid
$Pr = 0.005$	$Gr_{cr} \times 10^{-6}$	1.528	1.635	1.633	1.640	1.640	1.858	< 2.0
	f_{cr}	1132	1165	1163	1165	1166	—	1360
$Pr = 0.015$	$Gr_{cr} \times 10^{-6}$	2.828	2.932	2.908	2.909	2.908	3.108	—
	f_{cr}	1364	1371	1369	1369	1369	—	—

TABLE 1. Convergence study and comparison with other independent calculations for $A = 1$.

		32×18 basis functions	40 × 30 basis functions	60 × 20 basis functions	60 × 24 basis functions	Ben Hadid & Roux (1990) 121 × 41 stretched FD grid	Pulicani *et al.* (1990) 40 × 30 Chebyshev spectral modes	Le Quere (1990) 50 × 20 Chebyshev pseudospectral modes	Winters (1988, 1990) 66 × 24 biquadratic finite elements	Present result 200 × 100 uniform finite-volume grid
$Pr = 0$	$Gr^*_{cr} = Gr_{cr}/A$	25520	25426	25417	25417	25000–25500	25000–25500	25350	25525	25000–27500
	f_{cr}	16.037	16.163	16.173	16.173	<16.34	16.31	16.08	16.207	1602–17.02
$Pr = 0.015$	$Gr^*_{cr} = Gr_{cr}/A$	33095	33021	32996	32996	32500–33500	33300	—	33002	32500–33500
	f_{cr}	19.678	19.657	19.648	19.648	19.06–20.0	19.675	—	19.656	19.42–20.01

TABLE 2. Convergence study and comparison with other independent calculations for $A = 4$. Branch with a single convective circulation.

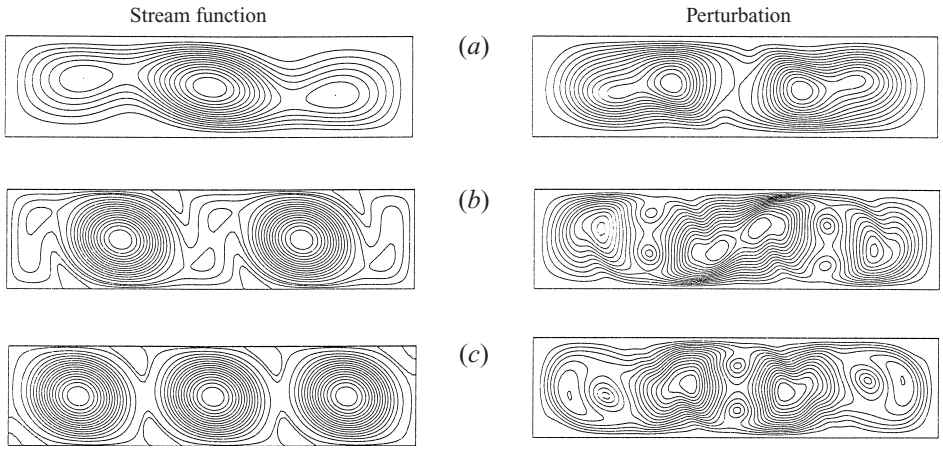

FIGURE 1. Streamlines and the corresponding perturbations of different branches of steady-state flows existing at $Pr = 0$, $A = 4$. (*a*) $Gr = 1.0 \times 10^5$. (*b*) $Gr = 3.7 \times 10^5$. (*c*) $Gr = 3.9 \times 10^5$.

§4). Depending on the governing parameters and the initial state, there can be three different steady-state flows with one, two, or three primary circulations (figure 1). All steady-state flows are centrally symmetric (namely, with respect to rotation through 180° about the centre of the cavity). For the considered boundary conditions (4)–(6), this central symmetry is a common property of steady-state flows at subcritical Grashof numbers. Note that all circulations rotate in a clockwise direction (figure 1). The steady state with a primary convective circulation (with or without two secondary rolls inside it; see figure 1) was the main objective of the investigation in the GAMM benchmark (Roux 1990). The convergence of the critical parameters for this state, and the comparison with the most accurate calculations, are shown in table 2 (note that, for comparison with the results of the GAMM benchmark, the Grashof number has to be redefined as $Gr^* = Gr/A$). A sufficiently good result for this case has been obtained already with 32×18 basis functions, and is in good agreement with the four most representative independent calculations (table 2). However, this particular case is easy, since sufficiently good results are obtainable with coarse spatial discretization. A relatively low value of the non-dimensional critical frequency (compare the values of f_{cr} in table 2 with those in tables 1 and 3) permits use of relatively large timesteps when the instability is simulated, using straightforward time integration.

The case shown in table 2 was used for validation of the finite-volume solver. The present results for $Pr = 0$ and 0.015 are shown in the last column of this table. It is seen that a 200×100 uniform grid yields the correct intervals where both the critical Grashof number and the critical frequency are located. It is known that grids stretched near the boundaries provide better resolution for the considered case (Ben Hadid & Roux 1990). For flow patterns with two and three primary circulations (figures 1*b*, *c*) such stretching does not seem very useful. Accordingly, all calculations by the finite-volume method were carried out with uniform grids only. On the other hand, the Chebyshev polynomials used for the basis functions of the Galerkin method are known to provide good resolution of the boundary layers and a high rate of convergence (Xin & Le Quere 1995). Thus, good agreement between the two independent numerical approaches guarantees good resolution of the boundary layers as well.

The second steady-state branch with two convective co-rotating circulations was obtained by Crespo del Arco *et al.* (1989) and again by many other independent

calculations. This steady-state flow does not exist at low Grashof number and appears as a stable steady state when the Grashof number reaches a certain value $Gr = Gr_l^{(2)}$, which was interpreted by Skeldon, Riley & Cliffe (1996) as branching from a saddle-node bifurcation point. The flow loses its stability at an upper value $Gr = Gr_u^{(2)}$ owing to supercritical Hopf bifurcation (the result obtained in the present work; see § 4). These two Gr values are compared with some other independent calculations in table 3 for $Pr = 0$ and 0.015. Calculation of the exact value of $Gr_l^{(2)}$ is difficult because the two-circulation solution does not exist below this value of Gr. We checked it by applying the arclength continuation technique and could not continue the branch of this solution below $Gr_l^{(2)}$. We also verified that when $Gr_l^{(2)}$ is approached from above, the dominant eigenvalue tends to zero. To determine the correct value of $Gr_l^{(2)}$, the Grashof number was varied within its fifth digit. Table 3 shows that four digits of $Gr_l^{(2)}$ remain unchanged starting with 50×20 basis functions. The calculated value of $Gr_l^{(2)}$ is slightly below those obtained by Skeldon *et al.* for $Pr = 0$. This should be so, since their calculations were not exact and relatively large increments were used in finding the upper value of Gr, beyond which the stable steady-state solution with two circulations does not exist. $Gr_u^{(2)}$ is larger than $Gr_l^{(2)}$, and the convergence of the former is slower, but the two first digits remain unchanged starting with 60×20 basis functions (table 3). For $Pr = 0.015$, only calculations for perfect thermal conducting horizontal boundaries are available for comparison. It is seen that the $Gr_l^{(2)}$ and $Gr_u^{(2)}$ calculated for different boundary conditions at $Pr = 0.015$ are close, which indicates that the thermal boundary conditions imposed on the horizontal boundaries do not strongly affect the stability of the discussed steady state. The result of Estivalezes, Boisson & Kourta (1989) for $Gr_u^{(2)}$ and the corresponding critical frequency provides aditional validation of the present result. Weak dependence of the critical numbers on the thermal boundary conditions indicates that the instability is caused mainly by the hydrodynamic mechanisms and is not strongly affected by the convective heat transfer. In such cases, the onset of instability can be described by the limit of zero Prandtl number (see § 4.3).

Another stable steady-state flow existing at $A = 4$ and $Pr = 0$, and consisting of three convective co-rotating clockwise circulations (figure 1*c*), was calculated only by Ben Hadid & Roux (1990). The stability interval of this flow is very narrow: according to the present calculations, it becomes stable at $Gr_l^{(3)} \approx 3.7 \times 10^5$ and oscillatory-unstable at $Gr_u^{(3)} \approx 4.05 \times 10^5$ owing to a supercritical Hopf bifurcation. Convergence is practically achieved with 60×20 basis functions. The calculated value $Gr_l^{(3)}$ is in good agreement with the above result of Ben Hadid & Roux (1990), while the present value of $Gr_u^{(3)}$ is approximately half of theirs (their exact results are $Gr_l^{(3)} \approx 3.64 \times 10^5$ and $Gr_u^{(3)} \approx 8.0 \times 10^5$).

The values of the lower and upper critical Grashof numbers obtained in the present work for the steady-state flows consisting of two and three rolls can be considered as an extension of the GAMM benchmark. In addition, the isolines of the modulus of the most unstable perturbations are included in figure 1. These isolines describe the distribution of the average amplitude of slightly supercritical oscillations of the flow, which can be used as an additional qualitative comparison of different numerical results.

4. Results and discussion

The main objective of the present analysis is to obtain stability diagrams in the (Gr, A)-plane which show stability regions of all branches of the steady-state flows

https://doi.org/10.1017/S0022112099004796 Published online by Cambridge University Press

	50×20 basis functions	60×20 basis functions	70×30 basis functions	80×30 basis functions	90×20 basis functions	Ben Hadid & Roux (1990) 121×41 stretched FD grid	Pulicani *et al.* (1990) 40 × 30 Chebyshev spectral modes	Le Garrec & Magnaud (1990) 120×30 uniform FE grid	Winters (1990) 30×12 biquadratic finite elements	Estivalezes *et al.* (1989) 80×40 uniform finite-volume grid
						$Pr = 0$				
$Gr_l^{(2)} \times 10^{-5}$	0.97637	0.97640	0.97639	0.97639	0.97639	1.0	0.98	1.04	1.156	
$f_l^{(2)}$	0	0	0	0	0					
$Gr_u^{(2)} \times 10^{-6}$	0.399320	0.394179	0.395041	0.395308	0.395307					
$fu_u^{(2)}$	102.8	106.5	107.1	107.2	107.2					
						$Pr = 0.015$				
$Gr_l^{(2)} \times 10^{-6}$	0.12003	0.12003	0.12003	0.12003	0.12003	0.112*			0.115*	0.10*
$f_l^{(2)}$	0	0	0	0	0					
$Gr_u^{(2)} \times 10^{-6}$	1.500	1.517	1.470	1.485	1.478					1.6*
$f_u^{(2)}$	179.3	183.4	179.9	181.1	180.4					182*

*Calculations for perfectly conducting horizontal boundaries.

TABLE 3. Lower and upper critical parameters for the steady state with two convective circulations ($A = 4$).

found in the present work. The stability analysis was carried out separately for each branch with one, two, three, and four primary convective rolls. The diagrams allow us to understand which stable asymptotic states are possible for certain governing parameters, and when a transition from one branch to another can be expected. Additional attention is paid to the dependence of the critical parameters on the Prandtl number and to their asymptotic behaviour at large values of the aspect ratio.

The appearance of a roll-type structure of the flow in long but finite cavities was associated with the transverse-roll instability in the horizontal layer (see Wang & Daniels 1994, and references therein). Drummond & Korpela (1987) assumed that a roll-type structure of steady flows develops as a result of an imperfect bifurcation. Our calculations for long cavities ($A \sim 10$), however, show that such a structure can develop with the continuous change of a single-roll steady-state flow with continuously increasing Grashof number. This is similar to the appearance of Taylor vortices in cylindrical annuli of finite length (Benjamin & Mullin 1981) or to that of vortex breakdown in cylinder with a rotating lid (Gelfgat *et al.* 1996*a*). Another similarity between our predictions and the above case of Taylor vortices is the simultaneous coexistence of multiple steady-state flows differing by the number of convective rolls (Taylor vortices). When the aspect ratio and Grashof number exceed certain values, the pattern of the final steady state is determined not only by the governing parameters, but also by the initial conditions (see below). It is also shown at which points different steady-state branches merge, and how the initial conditions should be defined to arrive at a flow pattern with a certain number of rolls.

4.1. *Stability diagrams and patterns of flows at* $Pr = 0$

In addition to the steady state flows (figure 1) with one, two, and three primary circulations, a steady flow with four primary rolls was found for $A > 5.5$. The complete stability diagram for $Pr = 0$ is shown in figure 2 and includes the dependence of the critical Grashof number on the aspect ratio (figure 2*a*) and that of the frequency at the onset of oscillations (critical frequency, figure 2*b*). Some characteristic patterns of oscillatory flows are shown as insets in figure 2(*b*). The snapshots correspond to time intervals equal to a quarter of the period of oscillations and are arranged in a clockwise sequence. The curves $Gr_{cr}(A)$ and $\omega_{cr}(A)$ indicate several different modes of the most unstable perturbation, which replace each other at points where the $Gr_{cr}(A)$ curves have breaks. The critical frequency (defined by the imaginary part of the dominant eigenvalues) changes abruptly at these points.

Upper parts of the neutral curves (figure 2*a*) correspond to the onset of oscillatory instability. The dashed regions indicate the areas where steady-state flows with a broken central symmetry are stable. These non-symmetric flows appear as a result of steady pitchfork bifurcation of the symmetric steady flows and become oscillatory-unstable above the corresponding black symbols (figure 2*a*). The steady pitchfork bifurcation takes place at the lower borders of the dashed regions indicated by blank symbols. In the case of the one-, two-, and three-roll flows, this bifurcation is supercritical, and the lower stability boundary of the non-symmetric flows coincides with the corresponding curves for the symmetric flows. In the case of the four-roll flows, the pitchfork bifurcation is subcritical and the stability regions of the symmetric and non-symmetric flows overlap. Transitions from the symmetric to non-symmetric steady-state flows are described in detail in Gelfgat *et al.* (1998*c*).

Unlike the stability boundary of the single-roll steady-state flows (the curve denoted by open circles in figure 2*a*), the stability regions of the multi-roll flows are bounded both from above and from below. Their upper boundary corresponds to the oscillatory

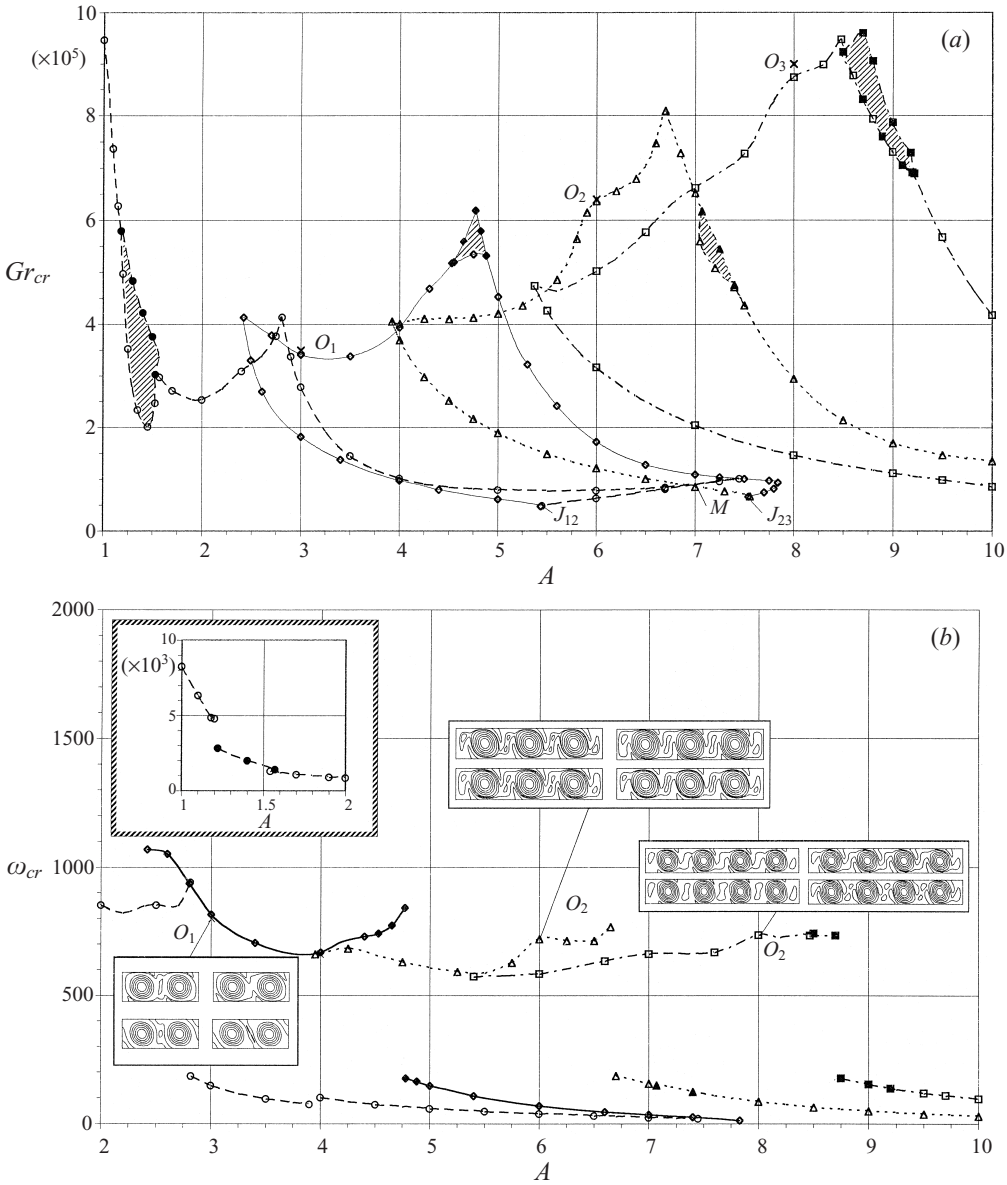

FIGURE 2. Stability diagram for $Pr = 0$. ○, flows with a single symmetric roll; ●, flows with a single non-symmetric roll; ◇, flows with two symmetric rolls; ◆, flows with two non-symmetric rolls; △, flows with three symmetric rolls; ▲, flows with three non-symmetric rolls; □, flows with four symmetric rolls; ■, flows with four non-symmetric rolls; ×, characteristic points discussed in the text. (*a*) Dependence of the critical Grashof number on the aspect ratio. (*b*) Dependence of the critical circular frequency on the aspect ratio.

instability of the steady-state flows, and the lower one, to a saddle-node bifurcation from one steady-state flow to another, or to an oscillatory flow with a different number of rolls.

Several stable steady-state flows can coexist in the areas where stability regions overlap. The final asymptotic state in this case depends not only on the governing

parameters but also on the initial state of the flow. An example of three different steady-state flows which are stable at the same values of the governing parameters corresponds to point M in figure 2(a). The corresponding flow patterns were reported by Gelfgat *et al.* (1998*a*). The coexistence of these three solutions was also validated by time-marching finite-volume calculations, for which the flows calculated by the Galerkin method were used as an initial guess. For three different initial guesses, the integration in time converged to the corresponding different steady states.

At low Grashof numbers, there exists only a unique single-cell steady-state flow. Therefore, with decrease of the Grashof number the multi-roll flows have to transform to a single-roll one. Moreover, there exist values of the aspect ratio at which (with decrease of the Grashof number) the flows with n and $(n+1)$ rolls become indistinguishable, and merge with each other and with the single-roll branch. Thus, the single-roll and two-roll states merge at point J_{12} (corresponding to the aspect ratio $A_{12} = 5.43$) in figure 2(a). Similarly, two-roll and three-roll states merge at point J_{23} which corresponds to the aspect ratio $A_{23} = 7.54$.

Transition from a single-roll to multi-roll flows takes place as follows. For $A < A_{12}$, with slow increase of the Grashof number up to onset of the oscillatory instability, the steady flow consists of a single primary convective roll. Conversely, a slow increase of the Grashof number in the interval $A_{12} < A < A_{23}$ leads to continuous development of two weak circulations inside the primary convective roll of a single-roll steady state. With still further increase of the Grashof number, these circulations grow, such that the steady-state flows continuously transform into a two-roll flow (figure 1b). A similar transition from a single-roll to a three-roll steady state happens in the interval $A_{23} < A < A_{34}(A_{34} > 10$ at $Pr = 0)$. The described transitions are continuous, and are not due to an imperfect bifurcation, as was interpreted by Drummond & Korpela (1987).

A computational route for obtaining a flow with a given number of rolls, according to the above results, can be described as follows: for a two-roll steady-state flow at $Pr = 0$, $A = 4$ and $Gr = 2 \times 10^5$, start from an aspect ratio inside the interval $5.43 = A_{12} < A < A_{23} = 7.54$ and slowly increase the Grashof number up to 2×10^5. The transition from a single-roll to a two-roll flow will then occur. Then, the aspect ratio should be slowly reduced to $A = 4$. The flow will preserve its two-roll structure. Steady states with other numbers of rolls can be obtained in a similar way. Note that values of A_{12} and A_{23} depend on the Prandtl number (see § 4.2).

Slightly supercritical oscillatory states with two, three, and four primary rolls correspond to points O_1, O_2 and O_3 in the insets of figure 2(b). Comparison of the patterns of the steady-state flows corresponding to the critical points, those of the perturbations (figure 1), and the snapshots of the slightly supercritical oscillatory states allows us to make an additional conclusion. As is seen in figure 1, in all these cases the maximal values of the perturbations (which correspond to the maxima of the oscillation amplitude) are located in the areas of relatively weak flows. In the case of the single-roll state (figure 1a) the maxima are located on the periphery of the primary convective roll. In the case of two and three rolls (figure 1b, c), the global maxima are located between the primary rolls. This indicates that the oscillatory instability is caused by a hydrodynamic interaction between the rolls. Note that for the case $Pr = 0$ considered in this section, the temperature is not perturbed at all. Hence, the instability is of purely hydrodynamic origin. As follows from the patterns of the perturbations, the oscillations of the streamlines are most noticeable between the primary rolls (see the insets in figure 2b) or outside a single primary roll. Similar patterns of perturbations and slightly supercritical oscillatory flows (not reported here) were also found for other values of the aspect ratio.

4.2. *Stability diagram and patterns of flows at* $Pr = 0.015$

The stability diagram for $Pr = 0.015$, shown in figure 3, is more complicated than that for $Pr = 0$, which indicates that convective heat transfer cannot be neglected for this small value Prandtl number. The dependence of the critical Grashof number on the aspect ratio for all four branches of the steady-state flows is shown in figure 3(a). To represent it with more details, the neutral curves of the stability diagram are also shown separately for the one- and two-roll flows in figure 3(b), and for the three- and four-roll flows in figure 3(c). Merging of the neutral curves at low Grashof numbers is shown in the inset of figure 3(a). Figure 3(d) shows the dependence of the critical frequency on the aspect ratio and corresponds to the neutral curves shown in figure 3(a). Snapshots of the streamlines of the oscillatory flows are illustrated in the insets in figure 3(b) and 3(c). Similarly to figure 2(b), the snapshots correspond to time intervals equal to a quarter of the oscillation period and are plotted in a clockwise sequence.

The characteristic points where the mode of the dominant perturbation changes, are denoted by lower case letters. This enables us to relate the curves $Gr_{cr}(A)$ and $\omega_{cr}(A)$ in figures 3(c) and 3(d). Roman letters from A to I correspond to the flows with three primary convective rolls, and italic letters from p to z correspond to those with four.

Similarly to the case of $Pr = 0$, the upper parts of the neutral curves in figures 3(a) to 3(c) correspond to transition from steady to oscillatory flow. Most of these transitions occur owing to Hopf bifurcation. Steady bifurcations (with $\omega_{cr} = 0$) were found for the two-roll flows in the interval $4.9 \leqslant A \leqslant 5.7$, and for the four-roll flows in the interval $8.77 \leqslant A \leqslant 10$ (branch of $Gr_{cr}(A)$ between points y and z in figure 3c). An integration in time was performed for several characteristic values from these intervals. It was found that in the interval $4.9 \leqslant A \leqslant 5.7$ the unstable symmetric two-roll flows transform into symmetric three-roll ones. In the interval $8.77 \leqslant A \leqslant 10$ the unstable symmetric four-roll flows transform into non-symmetric oscillatory four-roll ones. These steady bifurcations were not studied in detail. It can be interpreted that at $Pr = 0.015$ steady non-symmetric states are unstable, so that the described steady bifurcations lead either to another branch of the symmetric flows (in the interval $4.9 \leqslant A \leqslant 5.7$) or to oscillatory non-symmetric ones (in the interval $8.77 \leqslant A \leqslant 10$). Stable non-symmetric flows with one or three primary convective rolls were not found. An additional study is needed to find out for which parameters such non-symmetric flows are stable.

The lower branches of the neutral curves correspond to the saddle-node bifurcations from multi-roll to single-roll flows. Points where stability curves of the different branches merge are denoted as J_{12}, J_{23} and J_{34}. These points correspond to $A_{12} = 5.45$, $A_{23} = 7.5$ and $A_{34} = 10$, respectively.

Comparison of figures 2 and 3 shows that stability properties of the flows with small but finite Prandtl number ($Pr = 0.015$, figure 3) differ from those with zero Prandtl number (figure 2). Qualitative differences can also be seen in the patterns of the dominant perturbations (see also Gelfgat *et al.* 1998*a*, *b*). Dependence of the critical parameters on the Prandtl number will be discussed in § 4.3. There we also address some exceptional cases where a similarity between the onsets of the oscillatory instability at zero and small Prandtl numbers was found.

Steady states with two circulations are unstable inside the shaded areas in figures 3(a) and 3(b). This area lies inside the stability region of these flows. To check this unexpected result, unsteady calculations by the finite-volume method were carried out for a fixed value $A = 3.1$. The Grashof number was varied from the region of

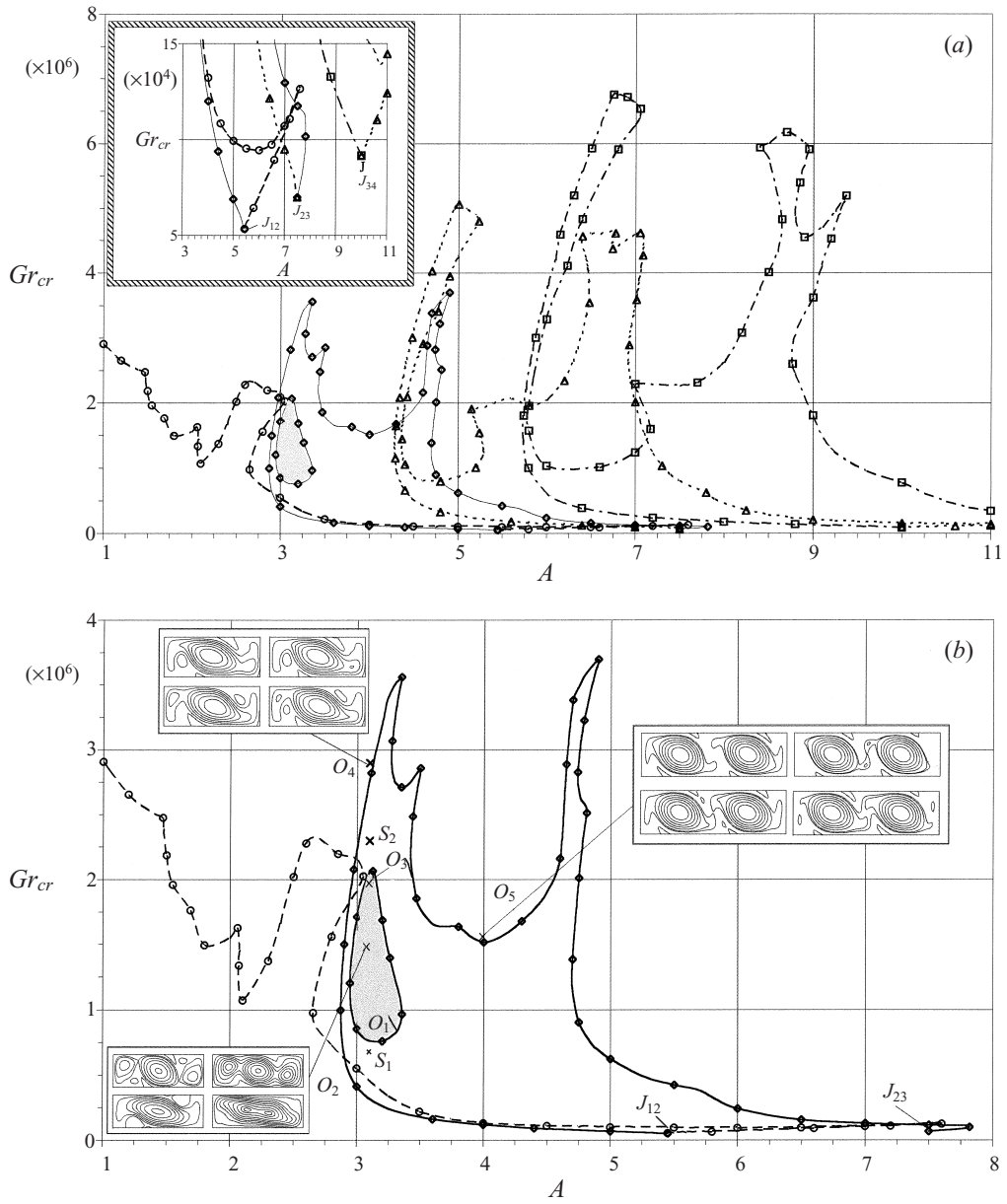

FIGURE 3 (*a,b*). For caption see facing page.

stable two-roll steady-state flows below the shaded area (point S_1 in figure 3*b*) up to the unstable region above the upper neutral curve (point O_4). The main purpose of this numerical experiment was to check whether direct numerical simulation will reproduce the same steady-state/oscillatory transitions, as was predicted by the linear stability analysis. The calculations, based on a 200×100 uniform grid with timestep 1.0×10^{-6}, were carried out for the points S_1, O_1, O_2, O_3, S_2 and O_4 in figure 3(*b*).

The numerical experiment proceeded as follows. First, a two-roll steady state at $Gr = 7 \times 10^5$ (point S_1 in figure 3*b*) was calculated. The steady solution, calculated by the Galerkin method, was used as an initial guess. Then, the Grashof number was

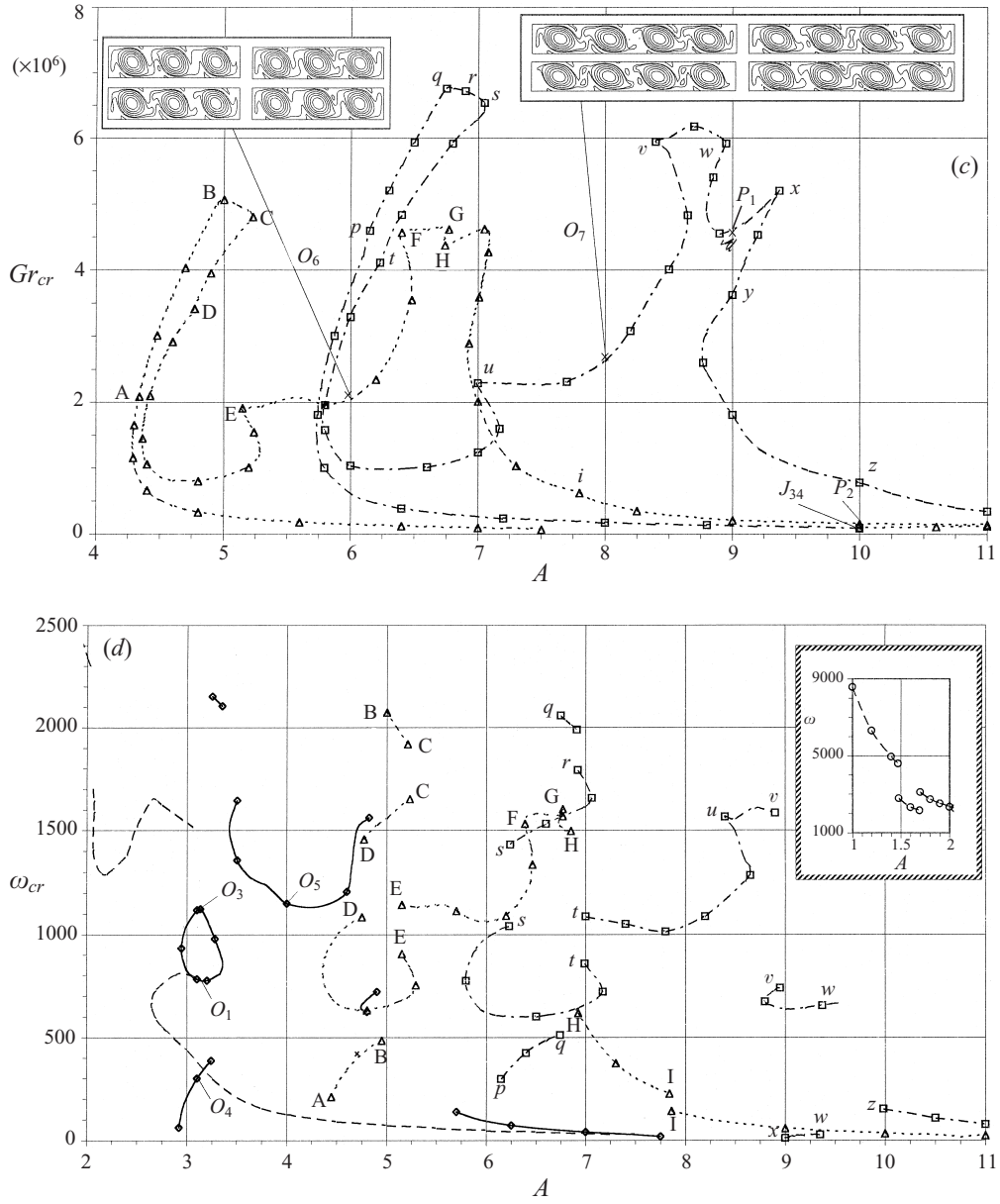

FIGURE 3. Stability diagram for $Pr = 0.015$ ○, flows with a single roll; ◇, flows with two rolls; △, flows with three rolls; □, flows with four rolls; ×, characteristic points discussed in the text. (*a*) Dependence of the critical Grashof number on the aspect ratio for four steady states. (*b*) Dependence of the critical Grashof number on the aspect ratio for single- and two-roll steady state flows. (*c*) Dependence of the critical Grashof number on the aspect ratio for three- and four-roll steady state flows. (*d*) Dependence of the critical circular frequency on the aspect ratio.

increased to $Gr = 8.1 \times 10^5$, slightly above the lower boundary of the shaded area (point O_1 in figure 3*b*). The flow became oscillatory with circular frequency $\omega = 786$, which agrees with the result of the Galerkin method $\omega_{cr} = 784$ (point O_1 in figure 3*d*). The frequency was determined using the self-sustained oscillations of the kinetic

energy in time. When the Grashof number was further increased up to $Gr = 1.5 \times 10^6$ (point O_2 and the corresponding inset in figure 3*b*) the two-roll oscillatory flow becomes unstable, and transforms into an oscillatory flow with a single roll. The oscillatory flow preserves the single-roll structure as the Grashof number continues to increase up to the upper boundary of the shaded area (point O_3 in figure 3(*b*), slightly below that boundary). If an oscillatory solution at $Gr = 2 \times 10^6$ is taken as an initial condition, and the Grashof number is further increased up to $Gr = 2.3 \times 10^6$ (point S_2 in figure 3*b*), which is inside the stability region of two-roll steady-state flows, the oscillatory single-roll flow transforms into a steady state with two rolls. Further increase of the Grashof number, beyond the upper boundary of the stability region, leads to onset of oscillatory instability, owing to a subcritical Hopf bifurcation, such that the unstable oscillations with two circulations transform into an oscillatory single-roll state. This final oscillatory state, corresponding to $Gr = 2.9 \times 10^6$ (point O_4 and the corresponding inset in figure 3*b*), is characterized by self-sustained oscillations of the kinetic energy at the frequency $\omega = 3300$.

The good agreement between the solution of the full unsteady problem and the results of the linear stability analysis should be considered as an additional validation of the latter. It should be emphasized that the two numerical techniques used here complement each other. Thus, for example, an unsteady calculation inside and outside the unstable shaded area (figure 3*b*) may be carried out only after this area has been found via the stability analysis. Conversely, transition from a two-roll steady-state flow to a single-roll oscillatory flow (points O_3 and O_4 in figure 3*b*) can be found only by means of the completely unsteady calculation.

As was mentioned in the previous section, oscillations of multi-roll flows are most noticeable between the primary convective rolls. A similar trend was found here. A two-roll oscillatory state is illustrated for point O_5 in figure 3(*b*). Three- and four-roll oscillatory states are illustrated in figure 3(*c*) for points O_6, O_7. All these steady/oscillatory transitions take place via a supercritical Hopf bifurcation.

4.3. *Dependence of critical parameters on the Prandtl number and comparison with experiments*

Several experiments, in which the onset of oscillatory instability in similar systems was studied, used the aspect ratio $A = 4$, with mercury ($Pr \approx 0.026$–0.027: Hart & Pratte 1990; Hung & Andereck 1990; Pratte & Hart 1990), gallium ($Pr \approx 0.017$–0.022: Braunsfurth & Mullin 1996), and indium–gallium–tin alloy ($Pr \approx 0.018$–0.019: Griaznov *et al.* 1989; Bojarevics, Gelfgat, Gorbunov 1992) as working liquids. The width ratio W (width/height) of the experimental containers varied from 1 to 5.5. Only flows with a single primary convective circulation were reported in all these experiments.

For better comparison with the experimental results, the dependence of the critical Grashof number on the Prandtl number was calculated for $A = 4$. The calculations were carried out for steady states with one primary circulation only, and for the interval $0.015 \leqslant Pr \leqslant 0.03$. The calculated stability diagram and the experimental data, available from literature, are shown in figure 4. The dependence $Gr_{cr}(Pr)$ becomes complicated when the Prandtl number exceeds 0.023 (figure 4*a*). There are three hysteresis loops of steady/oscillatory/steady transitions within the narrow interval, $0.023 < Pr < 0.027$. Such complicated behaviour of the neutral curve qualitatively reproduces the experimental graph $Gr_{cr}(Pr)$ of Braunsfurth & Mullin (1996) obtained for liquid gallium (see inset in figure 4*a*). Compared with the experimental data, the theoretically predicted interval is shifted towards larger values of Pr, and the upper

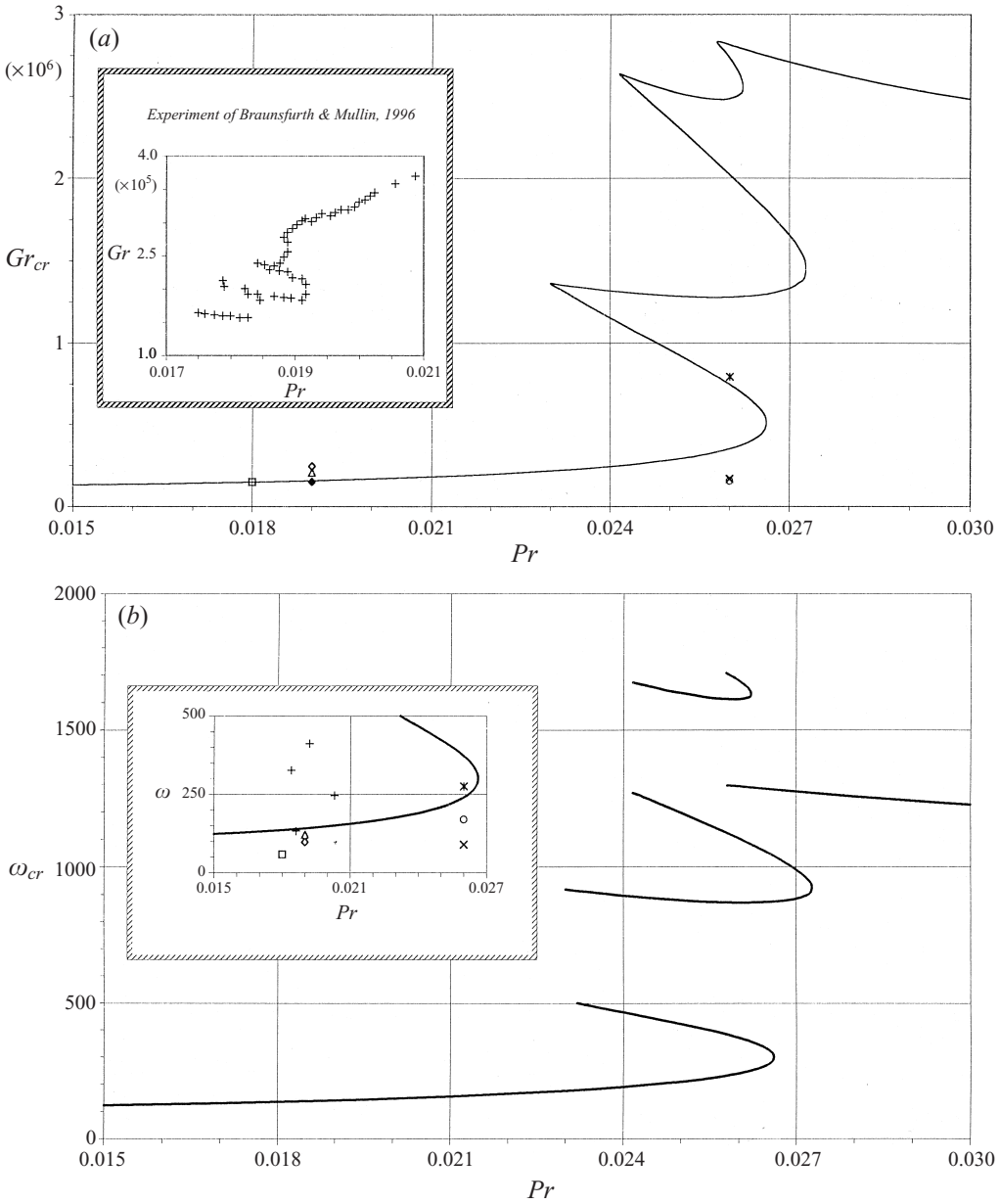

FIGURE 4. Stability diagram for the single-roll steady states at $A = 4$, and $0.015 \leqslant Pr \leqslant 0.03$. (*a*) Calculated dependence of the critical Grashof number on the Prandtl number and the experimental data available from literature (results of Braunsfurth & Mullin (1996) are shown in the inset). (*b*) Dependence of the critical circular frequency on the Prandtl number. ——, the present numerical result; ×, Hart & Pratte 1990, $4 \times 1 \times 1$; ✻, Hart & Pratte 1990, $4 \times 1 \times 2$; ○, Hung & Andereck 1990, $4 \times 1 \times 2$; □, Griaznov *et al.* 1990, $4 \times 1 \times 5.5$; △, Bojarevics *et al.* 1992, $4 \times 1 \times 5.4$; ◇, Bojarevics *et al.* 1992, $4 \times 1 \times 3.64$; ▽, Bojarevics *et al.* 1992, $4 \times 1 \times 2.5$; +, Braunsfurth & Mullin, 1996, $4 \times 1 \times 1$. (Non-dimensional sizes of the experimental containers are shown as: aspect ratio × height(=1) × width ratio.)

value of the critical Gr is larger than the experimental one. The difference may be due to strong three-dimensional effects (the width ratio in this experiment was $W = 1.1$), as well as to the temperature dependence of the Prandtl number (see Braunsfurth & Mullin 1996).

Experimental results should be compared with the lower branch of $Gr_{cr}(Pr)$ in figure 4(*a*). The corresponding comparison of the critical frequencies is shown in the inset of figure 4(*b*). The comparison shows that the experimental values of the critical Grashof number for the lower values of Pr($Pr = 0.018$ and 0.019) agree with the present two-dimensional calculations if the width ratio of the container is large enough. Thus, in the experiments of Bojarevics *et al.* (1992) and Griaznov *et al.* (1989) the critical Grashof numbers measured for $W > 5$ are very close to those calculated here (figure 4*a*). In the experiments of Bojarevics *et al.* (1992) the width ratio varied from $W = 2.5$ to $W = 5.4$, and it was concluded that as W increases, the critical Gr decreases, and the critical ω increases. It is also seen from figure 4 that as the width ratio increases, the experimental values of Gr_{cr} and ω_{cr} draw closer to the critical curves of the two-dimensional model. This indicates that the present two-dimensional study describes three-dimensional flows if the width ratio of the experimental container is sufficiently large. This assumption is supported also by the recent results of Gelfgat *et al.* (1998*c*), where experimental results of Pratte & Hart (1990), obtained for the container with $A = W = 8$ and $Pr = 0.026$, were reproduced by a two-dimensional numerical study.

As was mentioned above, the critical Grashof number, measured by Griaznov *et al.* (1989) for $W = 5.5$, is very close to Gr_{cr} calculated here. However, the experimental value of the critical frequency is about two times smaller than the present numerical result (figures 4*a*). A possible interpretation of this is a period-doubling bifurcation which may occur already at small supercriticalities.

The disagreement between the present two-dimensional numerical results and the experimental results of Hart & Pratte (1990) and Hung & Andereck (1990) (figure 4*b*) may have two reasons. The first is the smallness of the width ratio ($W = 1$ and 2) corresponding to these experiments. According to the results of Bojarevics *et al.* (1992), better agreement may be expected for width ratios beyond $W = 5$. The second reason is the Prandtl number of mercury ($Pr = 0.026$) which falls inside the hysteresis area (figure 4*a*). Since the shape of the neutral curve depends strongly on the width ratio, it can be expected that the shape and location of the hysteresis loops are strongly affected by the width of the experimental container. As was mentioned, this may be a good reason for the disagreement between the shape of the present neutral curve $Gr_{cr}(Pr)$ and the experimental one of Braunsfurth & Mullin (1996) (the width ratio in this experiment was $W = 1.1$).

It is known that, at $A = 4$, the onset of oscillatory instability of a single-roll flow is similar at $Pr = 0$ and $Pr = 0.015$, as was concluded by Gelfgat & Tanasawa (1994) after comparison of the patterns of the corresponding dominant perturbations. Because of this, the curve $Gr_{cr}(Pr)$ shown in figure 4(*a*) can be continuously extrapolated to $Pr = 0$. The similarity persists along the lower branch of the curve $Gr_{cr}(Pr)$ up to $Pr \approx 0.0266$, where the hysteresis loop begins. However, starting with $Pr \approx 0.023$ another perturbation pattern can be found at higher branches of the hysteresis loop.

Obviously, the location of the hysteresis loops of $Gr_{cr}(Pr)$ and the values of Pr, where modes of the dominant perturbations replace each other, depend on the aspect ratio. Therefore, whether similarity in the onset of oscillatory instability at zero and a certain small but finite Prandtl number exists should be checked for every particular value of the aspect ratio and for every particular branch of the steady-state flows. For

example, in the case $A = 1$, similarity between zero and very low finite Prandtl numbers exists up to $Pr \approx 0.0067$ (the corresponding stability diagram is not shown here).

4.4. *Asymptotic behaviour at large aspect ratios*

It was shown by Gelfgat *et al.* (1997) that in cavities with a stress-free upper boundary, there is no asymptotic behaviour at large aspect ratios (corresponding to an infinite fluid layer) up to $A = 10$, which means that, even at that value, flow in a finite cavity does not approach that in an infinite layer. The same is true with a no-slip upper boundary (see figures 2 and 3). However, some qualitative hints on the patterns and stability properties of flows in very long cavities can be extrapolated from the results obtained in the present work.

It is clear that as the aspect ratio increases, there exist stable steady-state flows with still larger numbers of primary convective rolls. Comparison of the neutral curves of steady-state flows with two, three and four rolls (figures 2(*a*) and 3(*a*)) shows a certain similarity in the shape of the stability regions. It is very likely that similar shapes exist for flows with five, six, and more primary rolls.

The patterns of the dominant perturbations corresponding to the oscillatory instability at $A = 9$ and 10 (not shown here) illustrate that the influence of the lateral boundaries cannot be neglected even at such high values of A. On the other hand, there is a certain similarity in the perturbation patterns of the stream function for a three-roll steady state at $A = 10$ and for the four-roll state at $A = 10$ (not shown here): two global maxima of the perturbations are located on the central roll in the three-roll state, and very similar maxima on the two rolls closest to the centre of the cavity in the four-roll one. This means that the rolls in the central part of the cavity are similarly perturbed. At the same time, the perturbation is weaker on the rolls located near the vertical walls. If this similarity persists for states with a larger number of primary rolls, then this instability corresponds to the infinite-layer case.

5. Conclusions

The main results obtained in the present work are:

1. The existence of multiple (two and more) steady states of the convective flow for $A > 2$ was shown and verified by two independent numerical approaches.

2. Regions of stability for each of the one-, two-, three-, and four-roll steady states were calculated for the intervals $0 \leqslant A \leqslant 10$ and $0 \leqslant A \leqslant 11$ for the two fixed values of the Prandtl number $Pr = 0$ and 0.015, respectively.

3. The neutral curve $Gr_{cr}(Pr)$ corresponding to the single-roll steady state was obtained for $A = 4$ and the interval $0.015 < Pr < 0.03$. Comparison with the experimental data (obtained for $A = 4$ and different Prandtl numbers) showed that the considered two-dimensional model can describe the experimentally observed instability onset if the width ratio of the experimental container is sufficiently large.

4. It was shown that the model with the neglected convective heat transfer (the case $Pr = 0$) cannot be a plausible approximation for description of stability of convective flows at small Prandtl numbers.

5. The stability analysis showed that the end effects cannot be neglected even for rather long cavities (with $A \sim 10$).

6. It was shown that, unlike the bifurcation to the transverse-roll flow in the infinite fluid layer (Nagata & Busse 1983; Kuo & Korpela 1988), a roll-type structure of convective flows in finite cavities can develop as a continuous change of the flow pattern.

7. Extrapolation of stability results to close values of the aspect ratio or Prandtl number is not always possible because of the complicated shape of the neutral curves.

8. There exist numerous modes of the dominant perturbations which abruptly replace each other when the governing parameters vary continuously. Therefore, various patterns of the oscillatory states can be expected. A common property of all slightly supercritical oscillatory states is strong oscillations between primary rolls and weak oscillations of the rolls themselves.

This work was supported by the German–Israeli Foundation for Scientific Research and Development (Grant no. I-284.046.10/93) and the Israel Ministry of Immigrant Absorption (to A. G.)

REFERENCES

Babu, V. & Korpela, S. A. 1994 Numerical solution of the incompressible three-dimensional Navier–Stokes equation. *Comput. Fluids* **23**, 675–691.

Ben Hadid, H. & Roux, B. 1990 Buoyancy-driven oscillatory flows in shallow cavities filled with low-Prandtl number fluids. In *Proc. GAMM Workshop on Numerical Solution of Oscillatory Convection in Low Prandtl Number Fluids* (ed. B. Roux). Notes on Numerical Fluid Mechanics, vol. 27, pp. 25–33. Vieweg, Braunschweig.

Benjamin, T. B. & Mullin, T. 1981 Anomalous modes in the Taylor experiment. *Proc. R. Soc. Lond.* A **377**, 221–249.

Bergman, T. L. & Ball K. S. 1994 Transition to oscillatory natural convection in low Pr liquids subject to a horizontal temperature gradient. *Proc. 10th Intl Heat Transfer Conf.* (ed. G. F. Hewitt), vol. 7, pp. 7–12. Brighton, UK.

Bojarevics, A., Gelfgat, Yu. M. & Gorbunov, L. A. 1992 Three-dimensional oscillatory convection of the low Prandtl number fluid in a rectangular cavity with different heating from the side (experiment). In *Proc. Ist Intl Symp. Hydrodyn. and Heat/Mass Transfer in Microgravity* (ed. V. S. Avduevsky), pp. 69–74. Gordon & Breach.

Braunsfurth, M. G. & Mullin, T. 1996 An experimental study of oscillatory convection in liquid gallium. *J. Fluid Mech.* **327**, 199–219.

Crespo del Arco, E., Pulicani, P. P. & Randriamampianina, A. 1989 Complex multiple solutions and hysteresis cycles near the onset of oscillatory convection in a $Pr = 0$ liquid submitted to a horizontal temperature gradient. *C. R. Acad. Sci. Paris* **309**, II, 1869–1876.

Drummond, J. E. & Korpela, S. A. 1987 Natural convection in a shallow cavity. *J. Fluid Mech.* **182**, 543–564.

Dupret, F. & Van der Bogaert, N. 1994 Modelling Bridgman and Czochralski growth. In *Handbook of Crystal Growth* (ed. D. T. J. Hurle) vol. 2, pp. 877–1010. North-Holland, Amsterdam.

Esposito, P. G. & Behnia, M. 1992 Numerical simulation of low Pr unsteady natural convection. *Proc. 11th Australian Fluid Mechanics Conf., Hobart, Australia* pp. 343–346.

Estivalezes, J. L., Boisson, H. C. & Kourta, A. 1989 Performances of the PISO algorithm applied to natural oscillatory convection in low Prandtl fluids. *Proc. 6th Intl Symp. On Numerical Methods in Laminar and Turbulent Flows, Swansea*, vol. 6, pp. 1023–1033.

Gelfgat, A. Yu., Bar-Yoseph, P. Z. & Solan, A. 1996*a* Stability of confined swirling flow with and without vortex breakdown. *J. Fluid Mech.* **311**, 1–36.

Gelfgat, A. Yu., Bar-Yoseph, P. Z. & Solan, A. 1996*b* Steady states and oscillatory instability of swirling flow in a cylinder with rotating top and bottom. *Phys. Fluids* **8**, 2614–2625.

Gelfgat, A. Yu., Bar-Yoseph, P. Z. & Yarin, A. L. 1997 On oscillatory instability of convective flows at low Prandtl number. *Trans. ASME* I: *J. Fluids Engng* **119**, 823–830.

Gelfgat, A. Yu., Bar-Yoseph, P. Z. & Yarin, A. L. 1998*a* Patterns of bifurcating convective flows in long horizontal cavities. *Advances in Computational Heat Transfer* (ed. G. de Vahl Davis & F. Arinc), pp. 403–410. Begell House, New York.

Gelfgat, A. Yu., Bar-Yoseph, P. Z. & Yarin, A. L. 1998*b* Multiplicity and stability of steady convective flows in laterally heated cavities. *Proc. 11th Intl Heat Transfer Conf. Kyongiu, Korea*, 23–28 August 1998, vol. 3, pp. 435–440.

Gelfgat A. Yu., Bar-Yoseph, P. Z. & Yarin A. L. 1998*c* Non-symmetric convective flows in laterally heated rectangular cavities. *Intl J. Comput. Fluid Dyn.* (in press).

Gelfgat, A. Yu. & Tanasawa, I. 1994 Numerical analysis of oscillatory instability of buoyancy convection with the Galerkin spectral method. *Numer. Heat Transfer* A **25**, 627–648.

Griaznov, V. L., Lebedev, A. P., Nikitin, S. A., Pavlovski, D. S. & Polezhaev, V. I. 1989 Thermal convection structure and temperature oscillations in semiconductor melts on earth and in microgravity. Theory and experiments. *Proc. 7th European Symp. Material and Fluid Sci. in Microgravity, Oxford*, 10–15 Sepetember 1989, pp. 231–236.

Hart, J. E. & Pratte, J. M. 1990 A laboratory study of oscillations in differentially heated layers of mercury. In *Proc. GAMM Workshop on Numerical Simulation of Oscillatory Convection in Low Prandtl Number Fluids* (ed. B. Roux) Notes on Numerical Fluid Mechanics, vol. 27, pp. 329–337. Vieweg Braunschweig.

Henry, D. & Buffat, M. 1998 Two- and three-dimensional numerical simulations of the transition to oscillatory convection in low-Prandtl-number fluids. *J. Fluid Mech.* **374**, 145–171.

Hung, M.-C. & Andereck, C. D. 1990 Subharmonic transitions in convection in a moderately shallow cavity. In *Proc. GAMM Workshop on Numerical Solution of Oscillatory Convection in Low Prandtl Number Fluids* (ed. B. Roux). Notes on Numerical Fluid Mechanics, vol. 27, pp. 338–343. Vieweg, Braunschweig.

Hurle, D. T. J. 1966 Temperature oscillations in molten metals and their relationship to growth striae in melt-grown crystals. *Phil. Mag.* **13**, 305–310.

Janssen, R. J. A., Henkes, R. A. W. M. & Hoogendoorn, C. J. 1993 Transition to time-periodicity of a natural convection flow in a 3D differentially heated cavity. *Intl J. Heat Mass Transfer* **36**, 2927–2940.

Kuo, H. P. & Korpela, S. A. 1988 Stability and finite amplitude natural convection in a shallow cavity with insulated top and bottom and heated from the side. *Phys. Fluids* **31**, 33–42.

Le Garrec, S. & Magnaud, E. D. 1990 Numerical simulation of oscillatory convection in low Prandtl number fluids. *Proc. GAMM Workshop on Numerical Solution of Oscillatory Convection in Low Prandtl Number Fluids* (ed. B. Roux), Notes on Numerical Fluid Mechanics, vol. 27, pp. 190–198. Vieweg, Braunschweig.

Le Quere, P. 1990 Contribution to GAMM workshop with a pseudo-spectral algorithm on a staggered grid. In *Proc. GAMM Workshop on Numerical Simulation of Oscillatory Convection in Low Prandtl Number Fluids* (ed. B. Roux). Notes on Numerical Fluid Mechanics, vol. 27, pp. 227–236. Vieweg, Braunschweig.

Monberg, E. 1994 Bridgman and related growth techniques. In *Handbook of Crystal Growth* (ed. D. T. J. Hurle), vol. 2, pp. 53–97. North-Holland, Amsterdam.

Müller, G. & Ostrogorsky, A. 1994 Convection in melt growth. In *Handbook of Crystal Growth* (ed. D. T. J. Hurle), vol. 2, pp. 711–781. North-Holland, Amsterdam.

Nagata, M. & Busse, F. H. 1983 Three-dimensional tertiary motions in a plane shear layer. *J. Fluid Mech.* **135**, 1–26.

Patankar, S. V. & Spalding D. B. 1972 A calculation procedure for heat, mass and momentum transfer in three-dimensional parabolic flows. *Intl J. Heat Mass Transfer* **15**, 1787–1806.

Pratte, J. M. & Hart, J. E. 1990 Endwall driven, low Prandtl number convection in a shallow rectangular cavity. *J. Cryst. Growth* **102**, 54–68.

Pulicani, J. P., Crespo del Arco, A., Randriamampianina, A. Bontoux, P. & Peyret, R. 1990 Spectral simulations of oscillatory convection at low Prandtl number. *Intl J. Numer. Methods Fluids* **10**, 481–517.

Roux, B. (ed.) 1990 *Numerical simulation of oscillatory convection in low-Pr fluids*: *A GAMM Workshop*. Notes on Numerical Fluid Mechanics, vol. 27. Vieweg, Braunschweig.

Skeldon, A. C., Riley, D. S. & Cliffe, K. A. 1996 Convection in a low Prandtl number fluid. *J. Cryst. Growth* **162**, 95–106.

Xin, S. & Le Quere P. 1995 Direct numerical simulations of two-dimensional chaotic natural convection in a differentially heated cavity of aspect ratio 4, *J. Fluid Mech.* **304**, 87–118.

Wang, T.-M. & Daniels, P. G. 1994 Numerical study of thermal convection in shallow cavities with conducting boundaries. *Intl J. Heat Mass Transfer* **37**, 387–399.

Winters, K. H. 1988 Oscillatory convection in liquid metals in a horizontal temperature gradient. *Intl J. Numer. Methods Engng* **25**, 401–414.

Winters, K. H. 1990 A bifurcation analysis of oscillatory convection in liquid metals. *Proc. GAMM Workshop on Numerical Solution of Oscillatory Convection in Low Prandtl Number Fluids* (ed. B. Roux). Notes on Numerical Fluid Mechanics, vol. 27, pp. 319–326. Vieweg, Braunschweig.